

High-Contrast Coronagraph Performance in the Presence of DM Actuator Defects

*Erkin Sidick, Stuart Shaklan, and Eric Cady

Jet Propulsion Laboratory, California Institute of Technology, 4800 Oak Grove Drive, Pasadena, CA 91109, USA

ABSTRACT

Deformable Mirrors (DMs) are critical elements in high contrast coronagraphs, requiring precision and stability measured in picometers to enable detection of Earth-like exoplanets. Occasionally DM actuators or their associated cables or electronics fail, requiring a wavefront control algorithm to compensate for actuators that may be displaced from their neighbors by hundreds of nanometers. We have carried out experiments on our High-Contrast Imaging Testbed (HCIT) to study the impact of failed actuators in partial fulfilment of the Terrestrial Planet Finder Coronagraph optical model validation milestone. We show that the wavefront control algorithm adapts to several broken actuators and maintains dark-hole contrast in broadband light.

Key words: Coronagraphy, adaptive optics, high-contrast imaging, space telescopes, exoplanets

1. INTRODUCTION

This paper presents both simulated and measured results on the sensitivity of broadband contrast to several failed actuators in a Lyot coronagraph implemented on the High-Contrast Imaging Testbed (HCIT) at NASA's Jet Propulsion Laboratory (JPL). This testbed is the Exoplanet Exploration Program's primary platform for experimentation [1-3]. It is used to provide laboratory validation of key technologies as well as to demonstrate a flight-traceable approach to implementation. It employs a 48x48 actuator deformable-mirror (DM) and a broadband wavefront correction algorithm called Electric Field Conjugation (EFC) to obtain the required 10^{-10} contrast [4]. In an effort to be able to predict the measured contrast performance of the coronagraph, we have carried out simulations by using the measured microscope image of an occulter's transmittance while keeping its phase the same as that of the model, as well as adding some phase values to the measured occulter spots. The laboratory testing was carried out with either a 2%-narrowband or a 10%-broadband light. The simulations were conducted with MACOS (Modeling and Analysis for Controlled Optical Systems) [5], and their results were compared with measurements. We achieved good agreement between the measurement and the simulation in some of the cases investigated. In four earlier papers we reported on the broadband contrast sensitivity to the number and the position of dead actuators, beam walk due to translation of a flat optic in the beam, as well as on the effects of occulter displacement, an opaque spot on the occulter, the controlled dark-hole dimensions, and the various defects of the focal plane mask [6-9]. In a companion paper, we will report the results of our simulations and experiment on the sensitivity of the broadband contrast to dark-hole size as well as control band [10]. In this paper we report our simulation and test results about the effects of one to four pairs of pegged (or frozen) DM actuators on the broadband contrast. In addition to comparing measured and simulated results for the above cases, we present additional simulation results for the cases that involve single pegged actuator as wells as a variety of other different actuator height values of the pegged actuators. The latter will help us to gain more comprehensive understanding about the impact of a special type of actuator failure mode, i.e. pegged actuators, on the broadband contrast.

2. DEFINITION OF DARK-HOLE AREA AND MEASURED CONTRAST MAPS

The detailed background information of the Lyot coronagraph used in this study is given in Ref. [7] as well as in our earlier papers, so it is not repeated here. For the current optical system with only one DM, we carry out wavefront control (WFC) over a region Ω_b , where Ω_b is a D-shaped dark-hole region bound by $X \geq X_{\min}$ and $R \leq R_{\max}$ with

*Erkin.Sidick@jpl.nasa.gov; Phone 1 818 393-7585; Fax 1 818 393-3290; www.jpl.nasa.gov

$X = x/f$, $Y = y/f$, $R = \sqrt{X^2 + Y^2}$, x and y are the horizontal and the vertical position variables on the corresponding image-plane, and f is the focal length. For example, in the current studies on the sensitivity of broadband contrast to pegged actuators, we used $[X_{\min}, R_{\max}] = [3.5 \ 11]\lambda/D$ for Ω_b . We evaluate the performance of the HCIT using the normalized intensity,

$$I_n(x, y) = I(x, y) / I_0, \quad (1)$$

where $I(x, y)$ is the image intensity of the occulted star, and I_0 is the maximum value of the un-occulted star intensity. We keep track of I_b , the mean value of $I_n(x, y)$ inside a ‘‘Big’’ dark-hole region Ω_b defined above.

3. RESULTS OF 1-4 PAIRS OF PEGGED ACTUATORS

In this test, actuators were offset significantly higher or lower from the nominal state used to minimize the optical system’s total wavefront error. This tests the ability of the wavefront control algorithm to recover from actuators that are ‘pegged’ near the end of their range of motion. **Figure 1** shows the DM’s nominal state actuator commands in nm.

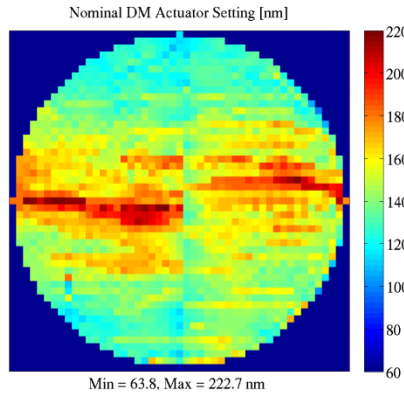


Figure 1. Nominal DM actuator heights in nm obtained when minimizing the overall wavefront error (WFE) through the system.

Software in the HCIT testbed protects the DM from potential damage caused by moving an actuator too far relative to its neighbors. This software limitation led us to move actuators in adjacent pairs such that the pair gave a 125 nm peak-offset in the wavefront in a localized region in the pupil. Without compensation by the EFC algorithm, a single pair of actuators in the clear aperture of the Lyot stop would cause a $\sim 5 \times 10^{-6}$ contrast change.

The experiment was run with 1, 2, 3 and 4-pairs of actuators poked, with the pokes alternating between introducing positive and negative OPD. After poking a pre-determined pair of actuators, EFC was run using 3-band control with the 2%-filters centered at 768, 800 and 832nm. Phase retrieval images were also taken for the DM setting before and after each run. Before carrying out broadband EFC simulations, we first determined the actual, post-EFC (experimental) heights of the pegged actuators from the phase-retrieval data. **Table 1** lists the intended and the actual heights of the pegged actuators and **Fig. 2** (top row) shows their locations. The actuator stroke amplitudes in the figure and in Table 1 are equivalent to one-half of the wavefront values. The second row of **Fig. 2** shows the post-EFC stroke amplitudes minus the nominal of **Fig. 1**. This corresponds to the change in wavefront that created the dark hole. The pegged actuators are shown at their measured positions. Our model results are in the 3rd and the 4th rows of **Fig. 2**. Starting from a flattened pupil (the condition that the nominal stroke amplitudes of **Fig. 1** create), a simulation that we refer to as ‘‘Sim1’’, the edge actuators around the Lyot stop move much less in the model than in the experiment. Curious to see if the model could find a good solution close to the experimental result, we also started with the experimental actuator stroke heights (row 2) and let EFC converge, leading to ‘‘Sim2’’ shown in row 4. Here there are significantly larger deviations from nominal than in the experiment. Thus the model does not accurately predict the DM settings around the pupil edge. However, it does accurately predict the behavior in the vicinity of the pegged actuators. **Figure 3** shows the

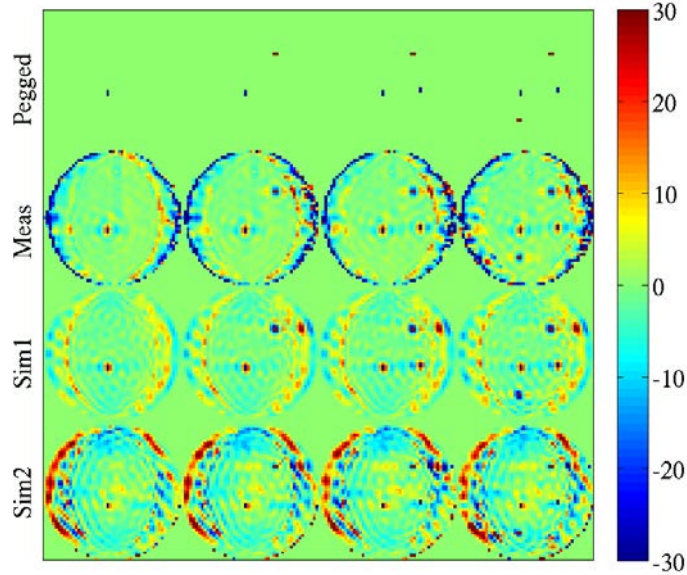


Figure 2. Top: Measured heights of the pegged actuators estimated from phase retrieval data after EFC had converged. Values are given Table 1. Second row: Measured heights of all actuators after EFC converged (relative to nominal condition of Fig. 1). Third row: Actuator heights from the model (the pegged actuator heights are fixed at the Table 1 values). We call this “Sim1”. They were obtained by setting the starting heights to zero for all actuators. Bottom: Actuator heights from the model (Sim2) when the starting actuator heights are the measured data of the second row. The color-stretch of the plot was truncated at $\pm 30\text{nm}$ to make more details of the actuator height maps visible.

Table 1. Intended and actual heights of the pegged actuators.

		1st Pair		2nd Pair		3rd Pair		4th Pair		Unit
Intended	All	-62.5	-62.5	62.5	62.5	-62.5	-62.5	62.5	62.5	nm
Actual	1-Pair	-66.5	-50.4							nm
	2-Pairs	-66.6	-50	65.8	55.9					nm
	3-Pairs	-65.8	-49.9	65.8	55.5	-49.4	-53.1			nm
	4-Pairs	-66.4	-49.9	65.8	55.6	-48.4	-52.5	55.1	55.1	nm

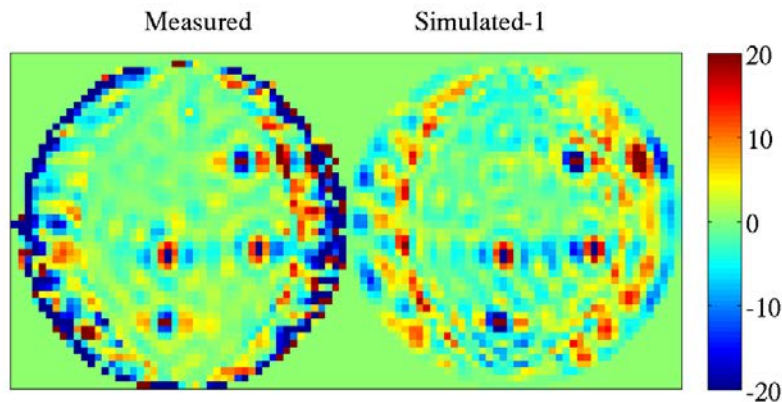


Figure 3. Measured and simulated (Sim1) actuator heights corresponding to 4-pairs of pegged actuators.

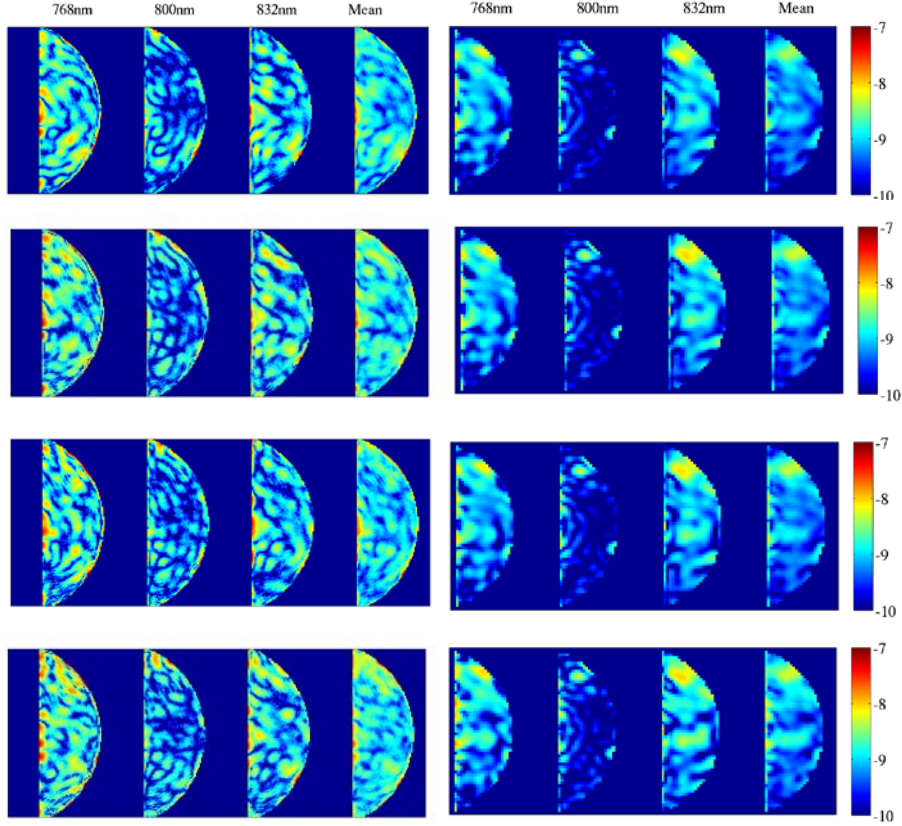


Figure 4. Left-column: Measured $I_n(x,y)$ maps at three 2%-bands and their mean inside a D-shaped dark-hole area with $[X_{\min}, R_{\max}] = [3.5 \ 11]\lambda/D$. From top to bottom they correspond to 1-, 2- 3- and 4-pairs of pegged actuators. Right-column: The corresponding simulated $I_n(x,y)$ maps obtained with monochromatic beams. The corresponding I_b values are plotted in Fig. 5. The simulated results were obtained starting EFC from a flat DM actuator state (Sim1).

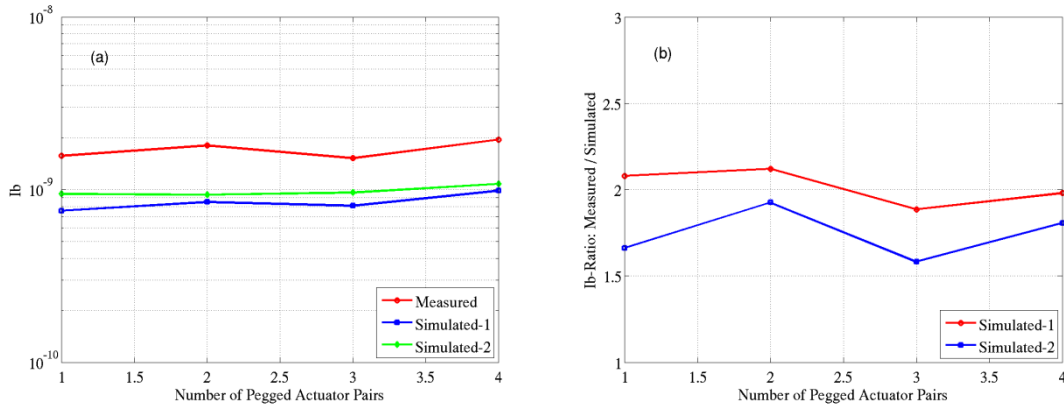


Figure 5. (a) Measured and calculated I_b values as a function of the number of the pegged actuator pairs. (b) The ratio of the measured and the simulated I_b values. The measured I_b values were calculated inside $[X_{\min}, R_{\max}] = [3.5 \ 10.6]\lambda/D$ because the EFC was carried out up to $R_{\max} = 11\lambda/D$ when using the 2%-filter centered at 768nm, and $R_{\max} = 11\lambda/D$ at 768nm becomes $R_{\max} = 10.6\lambda/D$ at the center wavelength of 800nm..

“zoomed-in” version of the measured and the simulated (Sim1) actuator heights corresponding to 4-pairs of pegged actuators. Note the compensatory negative and positive lobes around the pegged actuators.

The measured and the modeled dark hole images are shown in Fig. 4. We have used the mask OD map described in Ref. [9] (phase multiplier $F_{\text{spot}} = 1$) in these simulations. The corresponding I_b values and their measured-to-simulated ratios are plotted in Fig. 5. It is noted that the dependency of broadband contrast on the number of pegged actuator pairs is fairly weak.

4. RESULTS OF ADDITIONAL SIMULATIONS

In this section, we present some results on our additional simulations. Our goal is to gain a more comprehensive understanding about a special type of actuator failure mode, that is, pegged actuators. As we have seen from the results in the previous section, our simulations can predict the measured behavior of the broadband contrast fairly well. Therefore, we hope the simulated results to be presented below will fill some gaps that have not been considered in our tests.

4.1 Four-Pair Actuators Pegged: Nominal versus All-Positive and All-Negative Values

In Fig. 6 below we compared the $I_n(x,y)$ map of the nominal (alternating) 4-pair actuators pegged case with those of two new cases, that is, all 4-pairs of actuators are pegged by +62.5nm and -62.5nm. We included part (a), the case where no

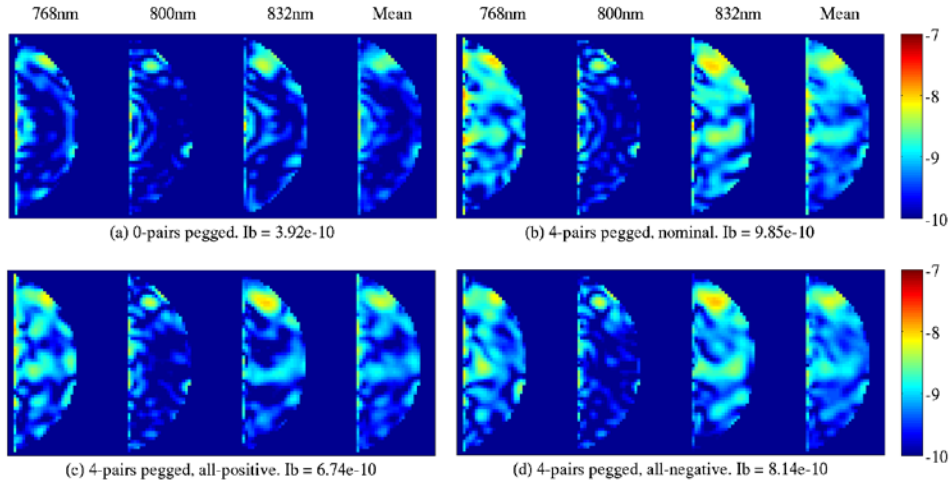


Figure 6. $I_n(x,y)$ maps at three monochromatic wavelengths and their mean corresponding to a D-shaped dark-hole area with $[X_{\text{min}}, R_{\text{max}}] = [3.5 \ 11]\lambda/D$. Part (a) corresponds to a case where no actuator is pegged. Part (b) is the same as the “4 alternating pairs pegged” in Fig. 4 (simulated), and the other two plots show the results of all-positive and all-negative pegging. The corresponding I_b value of the mean $I_n(x,y)$ map is listed in the x-label of each plot.

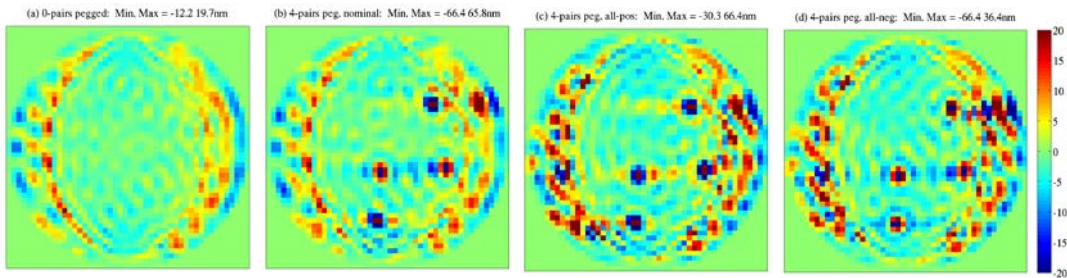


Figure 7. Actuator heights from the model. They were obtained by setting the starting heights to zero for all actuators (similar to “Sim1” in Fig. 2). No actuator is pegged in part (a). In Part (b), 4-pairs of actuators were pegged with values in Table 1. In parts (c) and (d), all 4-pairs were pegged by +62.5nm and -62.5nm, respectively. The color-stretch of the plot was truncated at $\pm 20\text{nm}$ to make more details of the actuator height maps visible.

actuator is pegged, as a reference. In Fig. 7 we show the corresponding DM actuator heights. When going from no faulty acutators to 4-pairs of pegged actuators, the mean contrast I_b rises to $7\text{-}9 \times 10^{-10}$. Also, pegging the actuators by all-positive and all-negative values improves the contrast relative to the nominal case, but only slightly. The actuators near the left and the right vertices work harder in the case of all-positive and all-negative pegging as compared to the nominal case, but the changes in the heights over the rest of the DM are relatively small.

4.2 Zero and 1 Actuator Pegged versus Others

We added two more cases to the simulated results presented in Section 3, that is, zero- and 1-pegged actuator. In the latter case, we chose one actuator in the location of the first actuator of the first-pair in Fig. 2, and set its height to negative 62.5nm. After including the broadband mean contrast results of these new cases to the original data set, Fig. 5(a) becomes as Fig. 8(a). The measured value of $I_b = 7.47 \times 10^{-10}$ corresponding to $N_{\text{peg}} = 0$ was obtained from Fig. 1(b) of Ref. [9]. The simulated results in this plot correspond to Sim1, and the results of Sim2 are not included in this plot. Both the measured and the simulated I_b values increase when the number of the pegged actuators, N_{peg} , is increased from zero to 2, and does not change much after that. Fig. 8(b) shows the post-EFC actuator heights obtained when only one actuator is pegged. The actuator heights in this plot are very similar to those of the $N_{\text{peg}} = 0$ case everywhere except at the location of the pegged actuator and its vicinity.

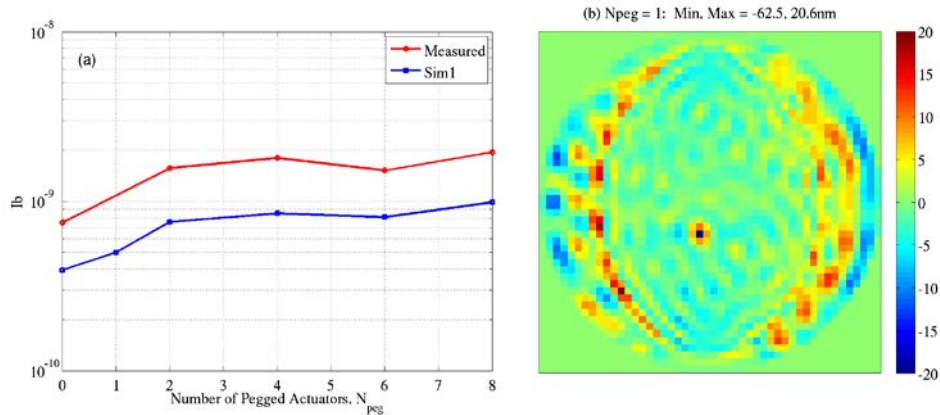


Figure 8. (a) Measured and predicted (Sim1) I_b values as a function of the pegged actuator number. (b) Actuator heights from the model corresponding to the case of 1-actuator is pegged, or $N_{\text{peg}} = 1$, with a value of -62.5nm. The color-stretch of the plot was truncated at $\pm 20\text{nm}$ to make more details of the actuator height maps visible.

4.3 Varying the Heights of Pegged Actuators

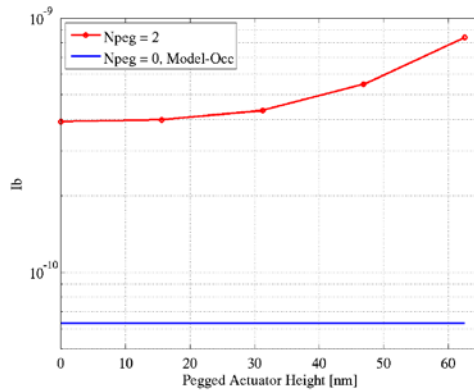


Figure 9. Predicted (Sim1) I_b values as a function of the pegged actuator height. They were obtained with $N_{\text{peg}} = 2$ (the first pair) and $h_1 = h_2$, that is, with the same height for both pegged actuators. The blue curve represents the result of the model occulter, $h_1 = h_2 = 0\text{nm}$, and no particle contamination of the mask.

We examined the dependence of the broadband contrast on the heights of the pegged actuators by increasing the height of the first pair of actuators ($N_{\text{peg}} = 2$) from $h_1 = h_2 = 0$ to -62.5nm with an increment of $\Delta h = (62.5/4)\text{nm}$. The result is shown in Fig. 9, where we plotted I_b as a function of the pegged actuator height. The blue-line in this plot represents the I_b -value corresponding to $N_{\text{peg}} = 0$ and model occulter explained in Ref. [9] in connection with Fig. 2, and included here as a reference. The model occulter uses theoretical transmission amplitude, and includes a parasitic phase profile as well as phase and OD dispersion, but does not have occulter spots and spot phases. The red-curve in this plot can be represented by a cubic-polynomial function. The last data point of Fig. 9 is similar to the blue-curve data point at $N_{\text{peg}} =$

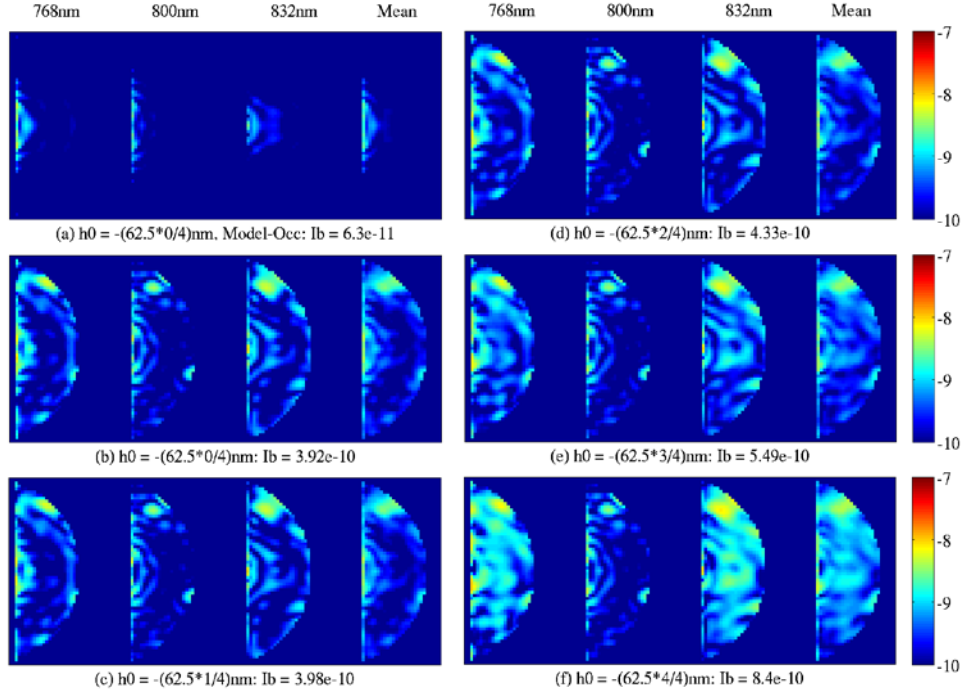


Figure 10. $I_n(x,y)$ maps at three monochromatic wavelengths and their mean corresponding to a D-shaped dark-hole area with $[X_{\min}, R_{\max}] = [3.5 \ 11]\lambda/D$. They were obtained with $N_{\text{peg}} = 2$ (the first pair) and $h_1 = h_2 = h_0$. The values of I_b and h_0 are given in the x-label of each plot. Part (a) was obtained with the model occulter and with $h_0 = 0\text{nm}$ and no mask contamination.

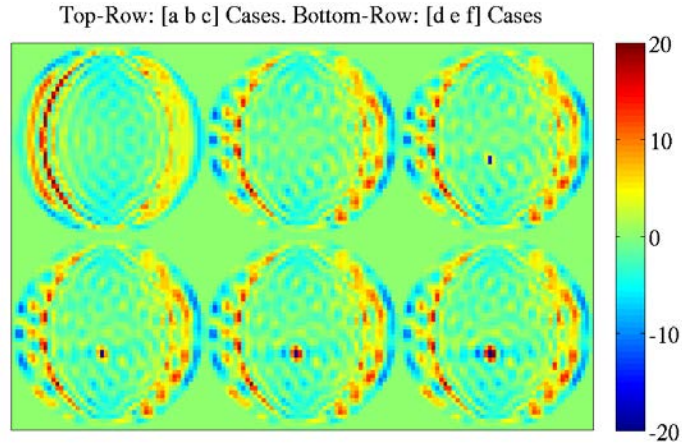


Figure 11. Actuator heights in nm corresponding to the six cases of Fig. 10. The color-stretch of the plot was truncated at $\pm 20\text{nm}$ to make more details of the actuator height maps visible.

2 in Fig. 8(a). The only difference is $h_1 = -66.5\text{nm}$ and $h_2 = -50.4\text{nm}$ in Fig. 8(a) and $h_1 = h_2 = -62.5\text{nm}$ in Fig. 9. The corresponding contrast values are $I_b = 7.55 \times 10^{-10}$ and 8.40×10^{-10} .

Figure 10 and Fig. 11 show the $I_n(x,y)$ maps and the actuator heights corresponding to the six cases in Fig. 9. As we can see from part (a) and part (b) of Fig. 10, the model occulter yields a I_b value about 6x better than the measured occulter. There are some differences in the corresponding actuator height maps as well. That is, the actuator height map of the model occulter has a slightly smoother pattern as compared to the measured occulter. And as in the five cases of the measured occulter, the DM actuator pattern does not change much with increasing value of the pegged actuator height except in the vicinity of the pegged actuators.

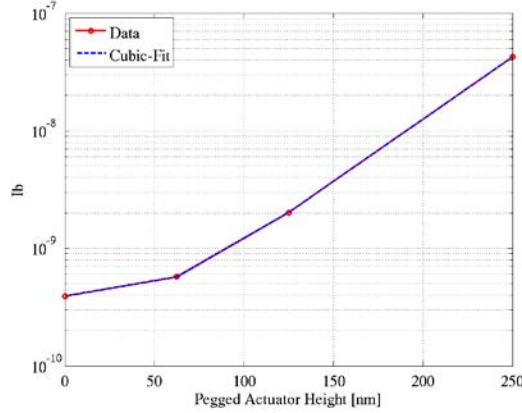


Figure 12. Simulated (Sim1) I_b values as a function of the pegged actuator height. They were obtained with $N_{\text{peg}} = 4$. That is, the first actuator was chosen from each pair in Fig. 3, and the heights of all four actuators were varied by the same amount while keeping their original signs.

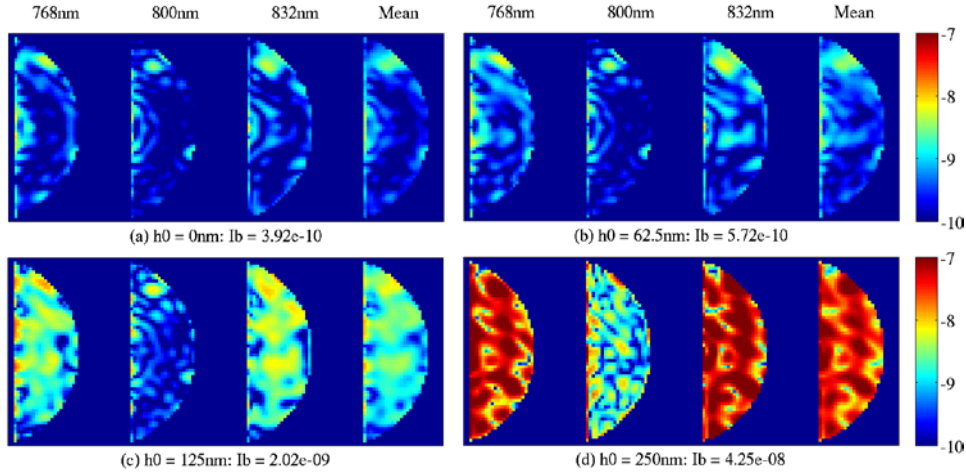


Figure 13. $I_n(x,y)$ maps at three monochromatic wavelengths and their mean corresponding to a D-shaped dark-hole area with $[X_{\text{min}}, R_{\text{max}}] = [3.5 \ 11]\lambda/D$. The four maps correspond to the four cases in Fig. 12, and h_0 given as x-label is the absolute value of the height of all four actuators.

As the next case of our investigation in this subsection, we chose four actuators ($N_{\text{peg}} = 4$), the first actuator of each pair from the 4-pair pegged actuator case (Fig. 3), and pegged them with the same actuator height value while keeping their original signs. We repeated this simulation for four different actuator height values. The obtained I_b values are shown as a function of the pegged actuator height in Fig. 12. The corresponding $I_n(x,y)$ maps and DM actuator heights are shown in Fig. 13 and Fig. 14.

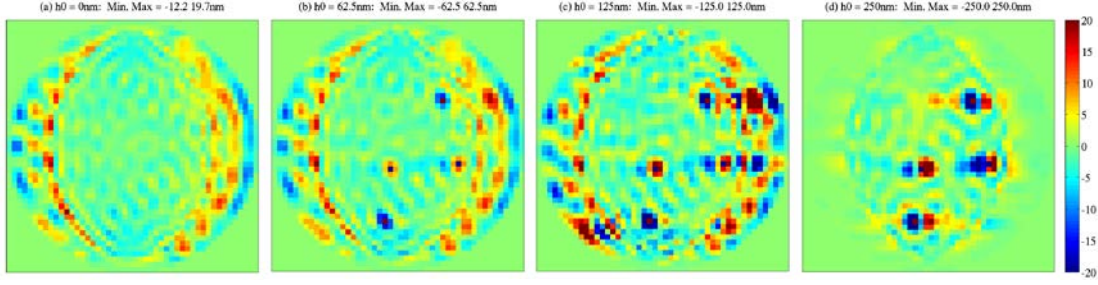


Figure 14. Actuator heights corresponding to the four cases in Fig. 12.

4.4 Model versus Measured Occulters

We can expect that the combined effects of occulter spots and spot phases will be reduced in the presence of pegged actuators. In order to gain some quantitative understanding in this regard, we pegged the 4-pairs of actuators in Fig. 2, either all negative (all-neg) or all positive (all-pos), with an absolute height value of $h_0 = 62.5\text{nm}$, and carried out EFC to obtain the best contrast possible. We did this simulation with the model occulter, and compared the results of $I_n(x,y)$ maps with those obtained with the measured occulter in Fig. 15. The corresponding DM actuator heights of the four different cases are shown in Fig. 16. When no actuator is pegged, the I_b value is degraded by about 6x when going from the model to the measured occulter, as shown in Fig. 10(a) and 10(b). But in the current pegged actuator case, that factor reduces to ~ 1.75 . The model occulter results in actuator height maps with smoother ring patterns as compared to the measured occulter (see Fig. 16).

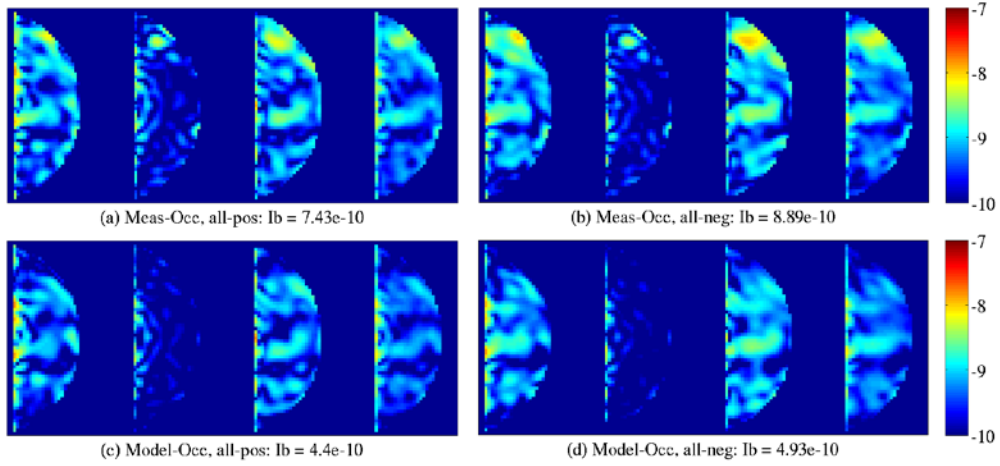


Figure 15. $I_n(x,y)$ maps at three monochromatic wavelengths and their mean corresponding to a D-shaped dark-hole area with $[X_{\min}, R_{\max}] = [3.5 \ 11]\lambda/D$. Parts (a-b) were obtained with the measured occulter by poking all 4-pairs of actuators with $h_0 = +62.5$ and -62.5nm , respectively, and parts (c-d) were obtained in a similar way but using the model occulter.

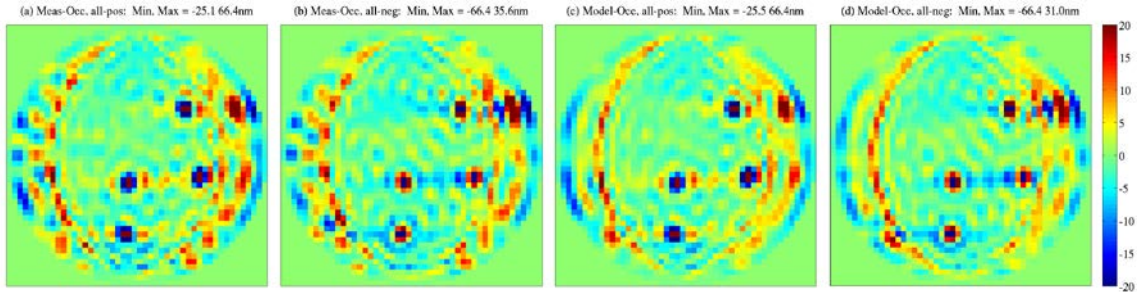


Figure 16. Actuator heights corresponding to the four cases in Fig. 15.

The actuator pegging patterns of Figs. 6(c-d) are identical to those of Figs. 15(a-b), but their I_b values are slightly different. This is because we used an “Actuator-regularization” method when obtaining the $I_n(x,y)$ maps in Figs. 6(c-d), and a “least-squares compensator with a tolerance” or a “pseudo-inverse” approach when obtaining Figs. 15(a-b) [11]. Our purpose here is to point out that all of the I_b values presented above are not unique. Different control approaches can result in slightly different I_b values. The use of different control steps or control parameters, such as different tolerance values or different actuator regularization factors in the same control algorithm, results in different I_b values. HCIT generally employs an “actuator-regularization” approach, but the control steps and control parameters are not unified among different researchers on the testbed as well as between measurement and simulations.

5. CONCLUSION

The behavior of the actuators of the deformable-mirrors (DMs) utilized on the HCIT testbed plays a crucial role in its contrast performance. In order to gain some general understanding about the potentials and the limitations of the current single-DM HCIT system, we have examined through actual tests as well as modeling and simulations the effects of one actuator error on the EFC-based control of the e-field over a half-dark hole region. Considered cases in experiment include one to 4-pairs of actuators that are ‘pegged’ near the end of their range of motion. In simulations we investigated several more cases to better understand the effect of this type of actuator failure mode on the broadband contrast. We have shown that our simulations can predict the broadband contrast behavior of the HCIT fairly well if we use the measured occulter transmission amplitude with its partially-transmitting spots (defects) as well as spot-OD dependent phases. In the cases of 1 – 4 pairs of actuators pegged with heights of $\sim 62.5\text{nm}$, we obtained measured-to-simulated broadband contrast ratios of ~ 2 , with the measured mean contrast being $I_b \sim 2 \times 10^{-9}$. When no actuator was pegged, we measured coherent 10%-broadband contrast of $I_b = 7.47 \times 10^{-10}$ [9].

In a companion paper we present results on our theoretical and experimental studies of the sensitivity of dark-hole contrast to the control bandwidth and dark-hole dimensions in our HCIT testbed [10]. We show good agreement between measurement and simulations in most cases, again assuming a model of phase-dependent mask defects.

The above experimental validations of key coronagraph sensitivity factors will additionally contribute to the confidence in performance prediction models for future flight systems.

This work was carried out at the Jet Propulsion Laboratory, California Institute of Technology, under contract with the National Aeronautics and Space Administration. Funding was provided through the 2010 Technology Demonstrations for Exoplanet Missions (TDEM) Strategic Astrophysics Technology proposal.

REFERENCES

- [1] John T. Trauger, Chris Burrows, Brian Gordon, Joseph J. Green, Andrew E. Lowman, Dwight Moody, Albert F. Niessner, Fang Shi, and Daniel Wilson, “Coronagraph contrast demonstrations with the high-contrast imaging testbed,” Proc. SPIE 5487, 1330 (2004).
- [2] Andrew E. Lowman, John T. Trauger, Brian Gordon, Joseph J. Green, Dwight Moody, Albert F. Niessner, and Fang Shi, “High-contrast imaging testbed for the Terrestrial Planet Finder coronagraph,” Proc. SPIE 5487, 1246 (2004).
- [3] Erkin Sidick, Fang Shi, Scott Basinger, Dwight Moody, Andrew E. Lowman, Andreas C. Kuhnert, and John T. Trauger, “Performance of TPF’s High-Contrast Imaging Testbed: Modeling and simulations,” Proc. SPIE 6265, 62653L (2006).
- [4] Amir Give’on et al, “Broadband wavefront correction algorithm for high-contrast imaging system,” Proc. SPIE 6691, 66910A (2007).
- [5] Modeling and Analysis for Controlled Optical Systems User’s Manual, Jet Propulsion Laboratory, California Institute of Technology, Pasadena, CA.
- [6] Erkin Sidick, Stuart Shaklan, Amir Give’on, and Brian Kern, " Studies of the effects of optical system errors on the HCIT contrast performance,” Proc. SPIE 8151, 8151-06 (2011).

- [7] Erkin Sidick, Stuart Shaklan, John Krist, Eric J. Cady, and Brian Kern, "HCIT contrast performance sensitivity studies: Simulation versus experiment," Proc. SPIE 8864, 88640Q-1 (2013).
- [8] Erkin Sidick, Stuart Shaklan, and Kunjithapatham Balasubramanian, "HCIT broadband contrast performance sensitivity studies," Proc. SPIE 8520, 85200M-1 (2012).
- [9] Erkin Sidick, Stuart Shaklan, Kunjithapatham Balasubramanian, and Eric Cady "High-contrast coronagraph performance in the presence of focal plane mask defects," Proc. SPIE 9143, 914336-1 (2014).
- [10] Erkin Sidick, Stuart Shaklan, and Eric Cady "Studies of the effects of control bandwidth and dark-hole size on the HCIT contrast performance," Proc. SPIE 9605, 9605-16 (2015).
- [11] Erkin Sidick, Scott A. Basinger, and David C. Redding, "An improved wavefront control algorithm for large space telescopes," Proc. SPIE 7015, 70154P (2008).